Letter

Antiferromagnetic insulators with tunable magnon-polaron Chern numbers induced by in-plane optical phonons

Bowen Ma [1,2,3] and Gregory A. Fiete [4,5]

[1]*Department of Physics, The University of Texas at Austin, Austin, Texas 78712, USA*
[2]*Department of Physics, The University of Hong Kong, Hong Kong, China*
[3]*HKU-UCAS Joint Institute of Theoretical and Computational Physics at Hong Kong, Hong Kong, China*
[4]*Department of Physics, Northeastern University, Boston, Massachusetts 02115, USA*
[5]*Department of Physics, Massachusetts Institute of Technology, Cambridge, Massachusetts 02139, USA*

(Received 29 August 2021; revised 7 February 2022; accepted 16 February 2022; published 3 March 2022)

We theoretically study magnon-phonon hybrid excitations (magnon polarons) in two-dimensional antiferromagnets on a honeycomb lattice. With an in-plane Dzyaloshinskii-Moriya interaction (DMI) allowed from mirror symmetry breaking from phonons, we find nontrivial Berry curvature around the anticrossing rings among the magnon and both optical and acoustic phonon bands, which gives rise to finite Chern numbers. We show that the Chern numbers of the magnon-polaron bands can be manipulated by changing the magnetic field direction or strength. We evaluate the thermal Hall conductivity reflecting the nontrivial Berry curvatures of magnon polarons and propose a valley Hall effect resulting from spin-induced chiral phonons as a possible experimental signature. Our study complements prior work on magnon-phonon hybridized systems without optical phonons and suggests possible applications in spin caloritronics with topological magnons and chiral phonons.

DOI: 10.1103/PhysRevB.105.L100402

Introduction. Antiferromagnetic materials have recently attracted a great deal of attention within the community of spintronics [1–3], because they are rather insensitive to the perturbation of magnetic fields and have small stray fields with fast THz magnetic dynamics compared to ferromagnets with frequencies in the GHz range. Research over the past decade has focused on spin dynamics and spin transport in antiferromagnets, which may originate from spin-transfer torques [4,5], domain-wall motion [6], and the spin Seebeck effect [7–9]. Magnons, as collective excitations emerging from magnetic order, have low dissipation and permit a pure spin transport without Joule heating, leading to a surge of interest in utilizing magnons for spintronics. Many magnonic analogs of electronic phenomena, such as the magnon thermal Hall effect [10–12], the magnon Nernst effect [13–15], and the magnonic Edelstein effect [16,17], have been theoretically studied and experimentally observed.

Along with magnonics, there is also a potential application in spintronics by combining magnetic orders with nontrivial band topology [18]. Topologically protected states are usually robust and only weakly affected by disorders. They can provide a high charge-to-spin conversion efficiency [19], exhibit strong magnetoresistance [20,21], and possess a number of exotic phenomena such as the quantum anomalous Hall effect [22,23] and chiral Majorana fermions [24]. In addition to fermionic topological excitations, there is also an emerging field of investigating topological bosonic excitations, such as topological magnons [25–28] and topological phonons [29–31]. Moreover, some recent works have shown topological properties in hybridized systems between magnons and acoustic phonons with magnetoelastic coupling [32–34], the Dzyaloshinskii-Moriya interaction (DMI) [35,36], and dipolar coupling [37]. However, a study of the coupling between magnons and optical phonons is still lacking.

In this Letter, we study hybrid magnon-phonon excitations in a two-dimensional (2D) collinear antiferromagnetic insulator (AFI) on the honeycomb lattice. The topological magnon bands originate from an in-plane nearest-neighbor DMI permitted by mirror symmetry breaking [38–40], which can be generically achieved in 2D van der Waals heterostructures, in the presence of magnon-phonon coupling. Since van der Waals antiferromagnets naturally possess at least two sublattices, it is possible to realize the coupling between magnons and optical phonons. In such a coupled magnon-(optical) phonon system, which has not been studied in the ferromagnetic case [35], we find nonzero Chern numbers with finite Berry curvatures and chiral phonons at high symmetry points [41,42].

We also show that the Chern numbers of magnon-polaron bands and the phonon chiralities can be manipulated by an external magnetic field. For connection to experiments, we evaluate the thermal Hall conductivity and propose a spin-induced valley Hall effect [42] as a possible experimental observation. We emphasize that our results are generic to many lattice structures and can be easily generalized to three-dimensional systems, as discussed at the end of this Letter. Our work suggests antiferromagnets with multiple sublattices—in contrast to ferromagnets—serve as promising platforms to realize tunable topological excitations hybridizing magnons with both acoustic and optical phonons, where the topology of the bands can provide robust information transport and may find possible applications in spintronics.

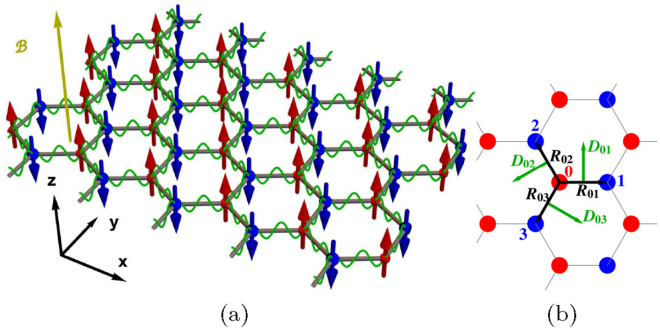

FIG. 1. (a) Schematic illustration of a hybrid magnon-phonon system. The ground state of the magnetization is Néel order along the z axis (red and blue arrows, color denoting the A and B sublattices). (b) DM vectors (green arrows) for the nearest bonds originated from mirror symmetry $\mathcal{M}_{yz}$ breaking.

Model. We consider a system with collinear AFI Néel order on a honeycomb lattice, where the magnetic moments are perpendicular to the plane, i.e., $\mathbf{S}_{A,B} = \pm S\hat{\mathbf{z}}$ for the A and B sublattices, respectively [see Fig. 1(a)]. The Hamiltonian describing both spin and lattice degrees of freedom can be written as $H = H_m + H_p + H_{mp}$, where the magnetic part H_m is given by

$$H_m = J_1 \sum_{\langle ij\rangle} \mathbf{S}_i \cdot \mathbf{S}_j - J_2 \sum_{\langle\langle ij\rangle\rangle} \mathbf{S}_i \cdot \mathbf{S}_j - \frac{K_z}{2} \sum_i \left(S_i^z\right)^2 - \mathcal{B} \sum_i S_i^z, \tag{1}$$

where J_1 (J_2) > 0 is the (next-) nearest-neighbor antiferromagnetic (ferromagnetic) Heisenberg exchange coupling, $K_z > 0$ is the easy-axis anisotropy, and $\mathcal{B} = g\mu_B B$ is the external effective Zeeman magnetic field. The phonon part H_p can be expressed as

$$H_p = \sum_i \frac{\mathbf{p}_i^2}{2M_i} + \frac{k_1}{2} \sum_{\langle ij\rangle} \left(\hat{\mathbf{R}}_{ij}^0 \cdot \mathbf{u}_{ij}\right)^2 + \frac{k_2}{2} \sum_{\langle\langle ij\rangle\rangle} \left(\hat{\mathbf{R}}_{ij}^0 \cdot \mathbf{u}_{ij}\right)^2, \tag{2}$$

where $\mathbf{u}_{ij} = \mathbf{u}_j - \mathbf{u}_i$ is the in-plane displacement of the lattice, $\hat{\mathbf{R}}_{ij}^0$ is the unit vector along bond ij in equilibrium, and k_1 (k_2) is the spring constant that corresponds to the elastic energy between two (next-) nearest-neighbor ions. Here, we ignore out-of-plane vibrations as they are higher-order terms [43].

For the magnon-phonon coupling H_{mp}, we begin from an in-plane nearest-neighbor DMI originating from mirror symmetry breaking. By Moriya's rule [44,45], the direction of the DM vectors is perpendicular to the bond, i.e., $\mathbf{D}_{ij} \propto \hat{\mathbf{z}} \times \mathbf{R}_{ij}$ [see Fig. 1(b)]. The DMI Hamiltonian is then

$$H_D = \mathbf{D}_{ij} \cdot (\mathbf{S}_i \times \mathbf{S}_j). \tag{3}$$

This term is not included in Eq. (1) since it is well known that DM vectors perpendicular to spin moments do not appear in the linear spin-wave Hamiltonian [10,35,36] and we assume it does not appreciably change (i.e., the change is numerically small) the Néel ground state order as long as the exchange coupling and anisotropy is large enough. However, both the magnitude and direction of $\mathbf{D}_{ij}$ depend on $\mathbf{R}_{ij}$ and thus it couples lattice and spin degrees of freedom. To lowest order of $\mathbf{u}_{ij}$ and $\delta\mathbf{s}_i = \mathbf{S}_i - \langle\mathbf{S}_i\rangle$, Eq. (3) can be expanded in a partial mean-field form as [43]

$$\begin{aligned} H_{mp} &\approx \frac{DS}{a} \sum_{\langle ij\rangle} \mathbf{u}_{ij} \left[\mathcal{I}_2 - \hat{\mathbf{R}}_{ij}^0 \hat{\mathbf{R}}_{ij}^0\right] (\delta\mathbf{s}_{A,i} + \delta\mathbf{s}_{B,j}) \\ &= \frac{DS}{a} \sum_{\langle ij\rangle} \left(\hat{\mathbf{R}}_{ij}^0 \times \mathbf{u}_{ij}\right) \cdot \left[\hat{\mathbf{R}}_{ij}^0 \times (\mathbf{S}_{A,i} + \mathbf{S}_{B,j})\right], \end{aligned} \tag{4}$$

where $D = |\mathbf{D}_{ij}|$ is the magnitude of the DMI, $a = |\mathbf{R}_{ij}^0|$ is the bond length, $\mathcal{I}_2$ is the 2×2 identity matrix, $\hat{\mathbf{R}}_{ij}^0 \hat{\mathbf{R}}_{ij}^0$ is the Kronecker product between two $\hat{\mathbf{R}}_{ij}^0$'s, and $\delta\mathbf{s}_{A(B),i} = (S_{A(B),i}^x, S_{A(B),i}^y) = \mathbf{S}_{A(B),i} - (+)S\hat{\mathbf{z}}$. The second equation mimics a Rashba-type spin-orbital coupling [46,47] or a Raman spin-phonon interaction [30,48–50], which has been studied in topological aspects of spin or phonon systems.

It is clear from Eq. (4) that the DMI-induced magnon-phonon coupling breaks the combined symmetry of time reversal plus 180° rotation about an in-plane axis [51,52]. With magnetic fields, this symmetry breaking allows the existence of a thermal Hall effect [53], which is absent in a magnon-only or phonon-only scenario. Moreover, in contrast to the ferromagnetic case, $H_{mp} + H_m$ also breaks inversion symmetry [13] and gives rise to chiral phonons at high symmetry points [41,42], as will be shown below.

Band topology. As magnons and phonons are both bosons, one can treat them equivalently as magnon-polaron excitations and rewrite $H = H_m + H_p + H_{mp}$ to a generalized Bogoliubov–de Gennes (BdG) form as [43]

$$H_{\mathbf{k}} = \begin{bmatrix} \frac{1}{2}\tilde{H}_m(\mathbf{k}) & \tilde{H}_{mp}(\mathbf{k}) & 0 \\ \tilde{H}_{mp}^\dagger(\mathbf{k}) & \frac{1}{2}D(\mathbf{k}) & 0 \\ 0 & 0 & \frac{\mathcal{I}_4}{2M} \end{bmatrix}, \tag{5}$$

with representation $\mathbf{X}_{\mathbf{k}} = (a_{\mathbf{k}}, b_{\mathbf{k}}, a_{-\mathbf{k}}^\dagger, b_{-\mathbf{k}}^\dagger, \mathbf{u}_{\mathbf{k}}, \mathbf{p}_{-\mathbf{k}})^T$, where $a_{\mathbf{k}}$ ($b_{\mathbf{k}}$) is the A (B) sublattice magnon annihilation operator in a Holstein-Primakoff representation [54], S_A^+ (S_B^+) $= \sqrt{2S}a$ ($b^\dagger$), $\mathbf{u}_{\mathbf{k}}$ ($\mathbf{p}_{-\mathbf{k}}$) is a four-vector for two-dimensional displacements (momenta) of A and B sublattices, $\tilde{H}_m(\mathbf{k})$ [$\tilde{H}_{mp}(\mathbf{k})$] corresponds to Eq. (1) [Eq. (4)], and $D(\mathbf{k})$ is the dynamical matrix corresponding to Eq. (2). Under this representation, the bosonic commutator is written as

$$[\mathbf{X}_{\mathbf{k}}, \mathbf{X}_{\mathbf{k}}^\dagger] = g = \begin{bmatrix} \mathcal{I}_2 & & & \\ & -\mathcal{I}_2 & & \\ & & & i\mathcal{I}_4 \\ & & -i\mathcal{I}_4 & \end{bmatrix}, \tag{6}$$

and the eigenstates satisfy [55,56]

$$gH_{\mathbf{k}}|\psi_{n\mathbf{k}}\rangle = \sigma_{nn} E_{n\mathbf{k}} |\psi_{n\mathbf{k}}\rangle, \quad \langle\psi_{n\mathbf{k}}|g|\psi_{n'\mathbf{k}}\rangle = \sigma_{nn'}, \tag{7}$$

where $\sigma = \sigma_z \bigotimes \mathcal{I}_{6\times 6}$ stands for particle-hole space. With particle-hole symmetry, $E_{n\mathbf{k}} = E_{n+6,-\mathbf{k}}$ and thus we only plot the first six eigenvalues in Fig. 2 and others are redundant. Here, $S_z = \langle\psi_{n\mathbf{k}}^R|(-a_{\mathbf{k}}^\dagger a_{\mathbf{k}} + b_{\mathbf{k}}^\dagger b_{\mathbf{k}} + \mathbf{u}_{\mathbf{k}}^A \times \mathbf{p}_{-\mathbf{k}}^A + \mathbf{u}_{\mathbf{k}}^B \times \mathbf{p}_{-\mathbf{k}}^B)|\psi_{n\mathbf{k}}^R\rangle$ mediates both magnon spins and phonon polarizations [41].

In Fig. 2, there are gapped rings around $\mathbf{\Gamma}$ or $\mathbf{K}$ ($\mathbf{K}'$) formed by anticrossing points among magnon and phonon

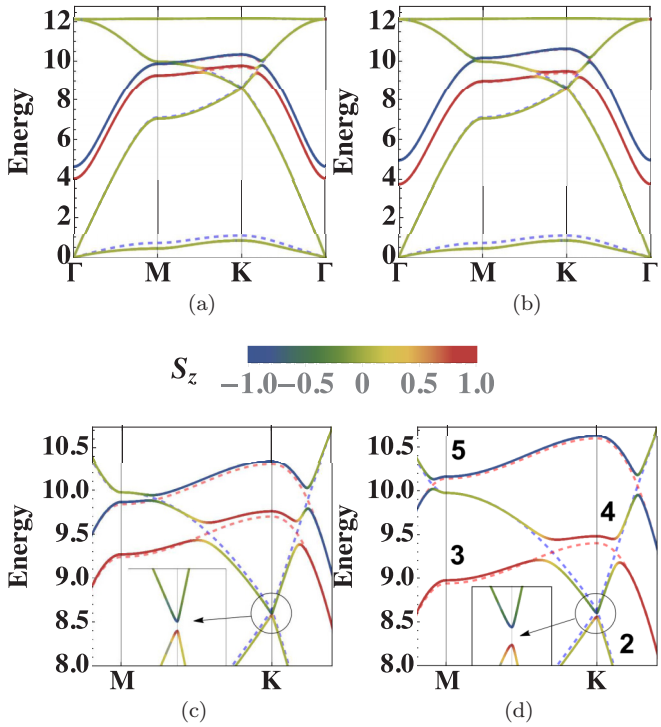

FIG. 2. Topological magnon-polaron bands. Energy is in meV. We set parameters as $S = 3/2$, $J_1 = 2.0\,\text{meV}$, $J_2 = 0.0\,\text{meV}$, $K_z = 1.0\,\text{meV}$, $m_B/m_A = 1$, $\hbar\sqrt{k_1/m_A} = 7.0\,\text{meV}$, $\hbar\sqrt{k_2/m_A} = 0.5\,\text{meV}$, $D = 0.2\,\text{meV}$. The blue (red) dashed lines are phonon (magnon) dispersions without DMI. The solid lines are magnon-polaron bands with DMI, where the color shows the z-component angular momentum, indicating whether the hybridization is more "magnonic" (as blue for $S_z = -1$ or red for $S_z = +1$) or "phononic" (as green for $S_z = 0$). (a), (b) Full band dispersions along the high symmetry path. (c), (d) Bands around anticrossing points. Band numbering is shown in (d). The insets show the gap opens at **K** and allows phonons with different chiralities (red or blue). Details are shown in Fig. 4. (a) $\mathcal{B} = 0.3\,\text{meV}$, (b) $\mathcal{B} = 0.6\,\text{meV}$, (c) $\mathcal{B} = 0.3\,\text{meV}$, and (d) $\mathcal{B} = 0.6\,\text{meV}$.

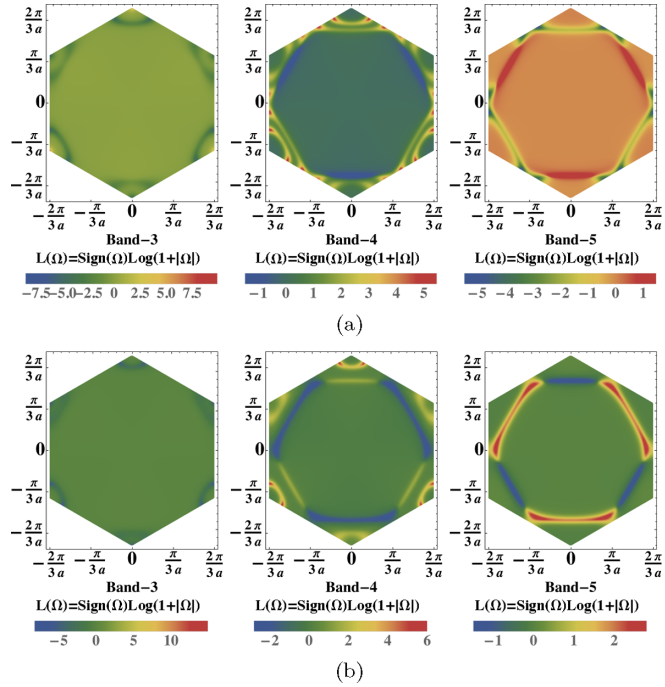

FIG. 3. Berry curvatures of the middle three anticrossed bands in Fig. 2. Band numbers are ordered from bottom to top. When the magnetic field increases, there is one gapped ring around **Γ** between bands 3 and 4 that splits into two rings around **K** and **K**′ leading to a topological phase transition. (a) $\mathcal{B} = 0.3\,\text{meV}$ and (b) $\mathcal{B} = 0.6\,\text{meV}$

bands due to the DMI coupling, which gives rise to nontrivial topological properties in this magnon-polaron system. In such a generalized BdG system, the Berry curvature is given by the Bloch wave function $|u_{n\mathbf{k}}\rangle = e^{-i\mathbf{k}\cdot\mathbf{r}}|\psi_{n\mathbf{k}}\rangle$ as [12,43] $\mathbf{\Omega}_{n\mathbf{k}} = i\langle\nabla_{\mathbf{k}}u_{n\mathbf{k}}|g\times|\nabla_{\mathbf{k}}u_{n\mathbf{k}}\rangle$, and the Chern numbers can be obtained by integrating Berry curvature $\Omega^z_{n\mathbf{k}}$ along the Brillouin zone as [57] $C_n = \frac{1}{2\pi}\int_{\text{BZ}} d^2\mathbf{k}\,\Omega^z_{n\mathbf{k}}$, from which we calculate the band Chern numbers [since the top (also bottom) two bands are degenerate at the **Γ** point, we add up the Berry curvature of the two bands to obtain a well-defined Chern number] by the Fukui method [43,58] and find that the magnetic field can change the Chern numbers by integers.

In Fig. 2(a), the Chern numbers for the middle three anticrossed bands from low to high are $(-2, +4, -2)$, while they change to $(-2, +1, +1)$ in Fig. 2(b) by a phase transition when $\mathcal{B} > \mathcal{B}_c$ ($\approx$0.41 meV with the parameters in Fig. 2 [43]). Since in this parameter region the coupling barely affects acoustic modes and the longitudinal optical (LO) mode, the band topology can be effectively mapped into an SU(3) algebra [34,59]. Here, instead of an analytic calculation (which is generally not accessible), we achieve an understanding of the band topology more intuitively by looking at the Berry curvatures.

As shown in Fig. 3, nontrivial Berry curvatures are induced around the anticrossing regions, and thus the change of Chern numbers can be intuitively understood as a pair of gapped rings around **K** and **K**′ combining into or split by one anticrossing ring around **Γ**. Notice that there are opposite Berry curvatures at **K** and **K**′ in band 3 from the gap by spin-induced inversion symmetry breaking, but it does not contribute to the Chern number due to a cancellation between these two valleys [42]. However, as shown in Figs. 4(a)–4(d), a large phonon angular momentum $S^z_P = \langle\mathbf{u}^A_{\mathbf{k}}\times\mathbf{p}^A_{-\mathbf{k}} + \mathbf{u}^B_{\mathbf{k}}\times\mathbf{p}^B_{-\mathbf{k}}\rangle$ occurs at **K** for bands 2 and 3 giving rise to chiral phonons. The polarization of these phonons can be flipped by reversing the magnetic field and they can contribute to a valley Hall effect [42].

Similar to the physics of gapped 2D Dirac systems [60], the physics of an anticrossing magnon-phonon pair can be effectively described by

$$H_{\text{eff}} = \frac{E^{\pm}_{m\mathbf{k}} + E^{\pm}_{p\mathbf{k}}}{2}\mathcal{I}_2 + \mathbf{d}^{\pm\pm}_{\mathbf{k}}\cdot\boldsymbol{\sigma} + V_{\mathbf{k}}, \tag{8}$$

where $E^{+(-)}_{m\mathbf{k}}$ is the upper (lower) magnon energy without the DMI, $E^{+(-)}_{p\mathbf{k}}$ is the transverse optical (longitudinal acoustic) phonon energy without the DMI, $\boldsymbol{\sigma} = (\sigma_x, \sigma_y, \sigma_z)$ are the Pauli matrices, $\mathbf{d}^{\pm\pm}_{\mathbf{k}}$ opens a gap between $E^{\pm}_{m\mathbf{k}}$ and $E^{\pm}_{p\mathbf{k}}$ arising from the DMI and can be regarded as an analog of the gaping term in the Kane-Mele model [61,62], and $V_{\mathbf{k}}$ includes terms that do not conserve particle numbers and perturbations that do not participate in opening the gap between the two

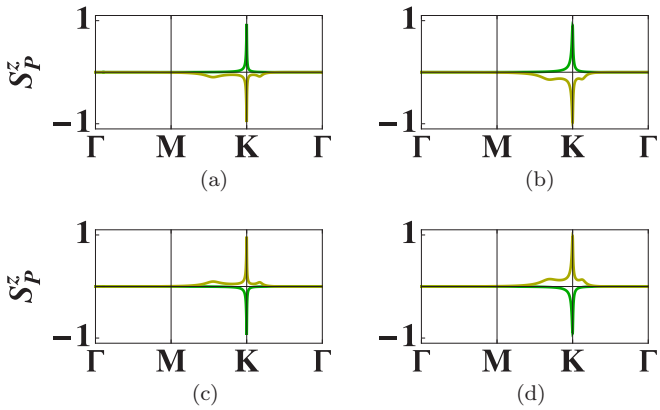

FIG. 4. Phonon polarization contribution $S_P^z = \langle \mathbf{u}_{\mathbf{k}}^A \times \mathbf{p}_{-\mathbf{k}}^A + \mathbf{u}_{\mathbf{k}}^B \times \mathbf{p}_{-\mathbf{k}}^B \rangle$ to S_z in Fig. 2. The green (yellow) line is for band 2 (band 3). The chiralities of phonons occur around **K**. (a) $\mathcal{B} = 0.3$ meV, (b) $\mathcal{B} = 0.6$ meV, (c) $\mathcal{B} = -0.3$ meV, and (d) $\mathcal{B} = -0.6$ meV.

bands [33,34]. A skyrmion (antiskyrmion) topological charge Q ($-Q$) can then be defined with $\mathbf{d}_{\mathbf{k}}^{\pm\pm}$ as $Q = \frac{1}{4\pi}\int d^2\mathbf{k}\, \hat{\mathbf{d}}_{\mathbf{k}} \cdot (\partial_{k_x}\hat{\mathbf{d}}_{\mathbf{k}} \times \partial_{k_y}\hat{\mathbf{d}}_{\mathbf{k}})$ for the upper (lower) band. In general, the analytical expression for $\mathbf{d}_{\mathbf{k}}^{\pm\pm}$ is not available, but since $\mathbf{d}_z^{\pm\pm} = (E_{m\mathbf{k}}^{\pm} - E_{p\mathbf{k}}^{\pm})/2$, the skyrmion numbers will change with the moving of anticrossing rings [33]. As the band Chern number reflects the winding number of $\hat{\mathbf{d}}_{\mathbf{k}}$ wrapping the unit sphere in the Brillouin zone, a skyrmion arising from $\mathbf{d}$ with charge Q determines the lower (upper) band with a Chern number Q ($-Q$) [63]. In addition to changing the field strength, reversing the external field will also change the Chern numbers by flipping the sign, thus we find the topology of our system is highly tunable.

Thermal and valley Hall effects. In order to connect our results with possible experimental observations, we evaluate the thermal Hall effect rising from the nontrivial Berry curvature of magnon-polaron bands. With a longitudinal temperature gradient $\nabla_y T$, an anomalous transverse motion of magnon-polaron excitations can be induced by the fictitious field $\Omega_{n\mathbf{k}}^z$ associated with a transverse thermal conductivity κ_{xy} as [12]

$$\kappa_{xy} = -\frac{k_B^2 T}{\hbar V}\sum_{n,\mathbf{k}}\left[c_2[g(E_{n\mathbf{k}})] - \frac{\pi^2}{3}\right]\Omega_{n\mathbf{k}}^z, \tag{9}$$

where $c_2(x) = (1+x)\ln^2(1+1/x) - \ln^2 x - 2\,\mathrm{Li}_2(-x)$, $\mathrm{Li}_2(x)$ is the polylogarithm function, and $g(x) = [\exp(x/k_BT) - 1]^{-1}$ is the Bose-Einstein distribution.

In Fig. 5, we evaluate κ_{xy} with parameters [64–66] for $MnPS_3$ as $m_A = m_B = M = 55$ u, $S = 5/2$, $J_1 = 1.54$ meV, $J_2 = 0.14$ meV, $g = -2.0$, and set $K_z = 0.1$ meV, $D = 0.5$ meV, $\hbar\sqrt{k_1/M} = 11$ meV, and $\hbar\sqrt{k_2/M} = 2.2$ meV. At the low field, the two magnon bands couple with the transverse optical (TO) phonon giving a Chern number distribution $(0, +2, -4, +2)$ from bottom to top, while they couple with the TO and longitudinal acoustic (LA) phonon, respectively, at high field giving a Chern distribution $(-2, +2, -2, +2)$. These results are also consistent with our analysis on band topology by looking at the moving of gapped rings. The change of κ_{xy} with magnetic field results from the topological transition with different Chern numbers, while the sign change

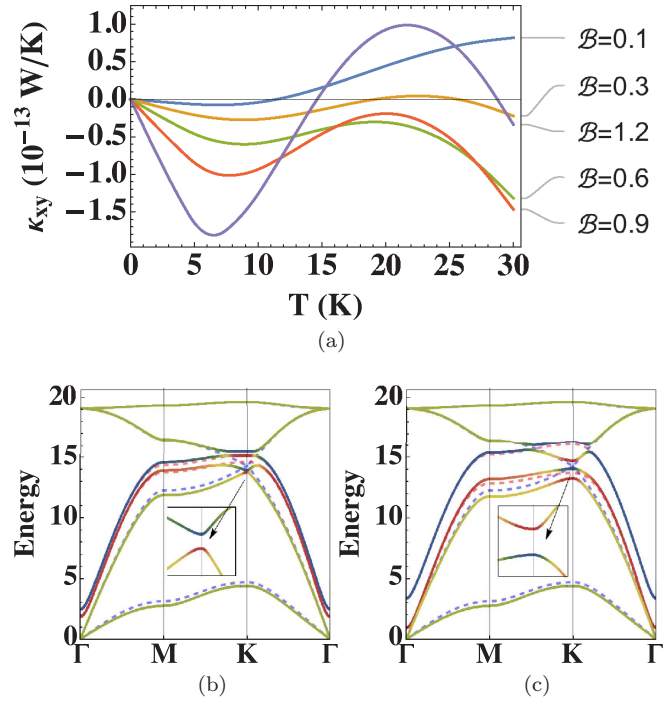

FIG. 5. (a) Thermal Hall response using parameters from $MnPS_3$. (b), (c) Band structures and Chern numbers for different external fields. See main text for details. (a) Thermal Hall response. $\mathcal{B}$ is in unit of meV, (b) $\mathcal{B} = 0.3$ meV with Chern number $(0,\ 0,\ -2,\ +4,\ -2,\ 0)$, and (c) $\mathcal{B} = 1.2$ meV with Chern number $(0,\ +2,\ -2,\ +2,\ -2,\ 0)$.

with temperature reflects the competition among bands of different Chern numbers which come to dominate the transverse thermal transport.

In addition, as the spatial inversion symmetry is broken by the spin degree of freedom, the gap opens at the **K** and **K**′ valley, and thus gives rise to chiral phonons with different polarizations at these high symmetry points [see Figs. 2(c), 2(d), 5(b), and 5(c)]. By introducing a longitudinal strain gradient across the system, we expect the opposite motion of chiral phonons at different valleys since $v \propto -\mathbf{E}_{\text{strain}} \times \mathbf{\Omega}$ in the transverse direction which creates a temperature difference between the two edges [42]. The sign of the valley Hall signal is also controllable by flipping the external magnetic field. As these two Hall effects originate from the nontrivial topology of the system, we expect to observe a thermal Hall signal only weakly affected by the bulk disorder.

Discussion. In this Letter, we study the topology of magnon-polaron bands in a 2D honeycomb Néel order antiferromagnet with an in-plane DMI induced by magnon-phonon coupling. Without the DMI, the magnon or phonon bands are trivial, while nontrivial Berry curvature occurs around the anticrossing rings opened by the magnon-phonon coupling. In contrast to previous studies on ferromagnetic magnons or on magnons coupled with only acoustic phonons, in our case, antiferromagnetic magnons can couple with both optical and acoustic phonons, giving rise to two remarkable results—highly tunable integer Chern numbers with an external magnetic field and the existence of chiral phonons. We also investigated a field-tunable thermal Hall effect induced

from the finite Berry curvatures and proposed valley Hall effects by spin-induced chiral phonons, both of which will generate significant experimental interests in the community.

Even though we study the model on a honeycomb lattice, the coupling can be expressed with a displacement field $\mathbf{u} \approx \mathbf{u}_{ij}/a$ and a staggered spin field $\mathbf{n} \approx (\mathbf{S}_A - \mathbf{S}_B)/2S$ as $\frac{DS^2}{a^3}(\nabla \times \mathbf{u}) \cdot (\nabla \times \mathbf{n})$ from Eq. (4), which does not depend on lattice details [43]. This is similar to Rashba spin-orbital coupling and the Raman spin-phonon interaction, revealing the underlying topological nature of this hybridized system. We believe this universal form is the key to the topology and gives a crucial insight that will be of interest to a broad community of researchers studying the consequences of magnon-phonon interactions. This 2D model can also be generalized to a 3D system with mirror symmetry breaking in the bulk [67,68] and it can couple the magnons with out-of-plane phonon modes as well which could further enrich the physics of topology. In principle, our method can be used in any bosonic system such as plasmonics [69,70] and photonics [71], and may find similar and interesting applications there. Our work opens another avenue in the study of hybridized magnon-phonon excitations by treating the optical and acoustic phonons on equal footing, and it may be useful to design tunable transport devices in the field of spintronics and draws a connection to chiral phonons with spin caloritronics.

Acknowledgments. We thank Nemin Wei and Naichao Hu for helpful discussions on band topology. We gratefully acknowledge support from NSF DMR-1949701 and NSF DMR-2114825, with additional support from the NSF through the Center for Dynamics and Control of Materials: an NSF MRSEC under Cooperative Agreement No. DMR-1720595. This work was performed in part at the Aspen Center for Physics, which is supported by National Science Foundation Grant No. PHY-1607611.

[1] T. Jungwirth, X. Marti, P. Wadley, and J. Wunderlich, Nat. Nanotechnol. **11**, 231 (2016).
[2] T. Jungwirth, J. Sinova, A. Manchon, X. Marti, J. Wunderlich, and C. Felser, Nat. Phys. **14**, 200 (2018).
[3] V. Baltz, A. Manchon, M. Tsoi, T. Moriyama, T. Ono, and Y. Tserkovnyak, Rev. Mod. Phys. **90**, 015005 (2018).
[4] R. Cheng, J. Xiao, Q. Niu, and A. Brataas, Phys. Rev. Lett. **113**, 057601 (2014).
[5] H. V. Gomonay and V. M. Loktev, Phys. Rev. B **81**, 144427 (2010).
[6] O. Gomonay, T. Jungwirth, and J. Sinova, Phys. Rev. Lett. **117**, 017202 (2016).
[7] S. M. Wu, W. Zhang, A. KC, P. Borisov, J. E. Pearson, J. S. Jiang, D. Lederman, A. Hoffmann, and A. Bhattacharya, Phys. Rev. Lett. **116**, 097204 (2016).
[8] Y. Ohnuma, H. Adachi, E. Saitoh, and S. Maekawa, Phys. Rev. B **87**, 014423 (2013).
[9] S. M. Rezende, R. L. Rodríguez-Suárez, and A. Azevedo, Phys. Rev. B **93**, 014425 (2016).
[10] H. Katsura, N. Nagaosa, and P. A. Lee, Phys. Rev. Lett. **104**, 066403 (2010).
[11] Y. Onose, T. Ideue, H. Katsura, Y. Shiomi, N. Nagaosa, and Y. Tokura, Science **329**, 297 (2010).
[12] R. Matsumoto and S. Murakami, Phys. Rev. B **84**, 184406 (2011).
[13] R. Cheng, S. Okamoto, and D. Xiao, Phys. Rev. Lett. **117**, 217202 (2016).
[14] V. A. Zyuzin and A. A. Kovalev, Phys. Rev. Lett. **117**, 217203 (2016).
[15] Y. Shiomi, R. Takashima, and E. Saitoh, Phys. Rev. B **96**, 134425 (2017).
[16] B. Li, A. Mook, A. Raeliarijaona, and A. A. Kovalev, Phys. Rev. B **101**, 024427 (2020).
[17] H. Zhang and R. Cheng, Appl. Phys. Lett. **117**, 222402 (2020).
[18] L. Šmejkal, Y. Mokrousov, B. Yan, and A. H. MacDonald, Nat. Phys. **14**, 242 (2018).
[19] H. Wang, J. Kally, J. S. Lee, T. Liu, H. Chang, D. R. Hickey, K. A. Mkhoyan, M. Wu, A. Richardella, and N. Samarth, Phys. Rev. Lett. **117**, 076601 (2016).
[20] X. Wang, Y. Du, S. Dou, and C. Zhang, Phys. Rev. Lett. **108**, 266806 (2012).
[21] T. Liang, Q. Gibson, M. N. Ali, M. Liu, R. Cava, and N. Ong, Nat. Mater. **14**, 280 (2015).
[22] C.-Z. Chang, J. Zhang, X. Feng, J. Shen, Z. Zhang, M. Guo, K. Li, Y. Ou, P. Wei, L.-L. Wang *et al.*, Science **340**, 167 (2013).
[23] Y. Deng, Y. Yu, M. Z. Shi, Z. Guo, Z. Xu, J. Wang, X. H. Chen, and Y. Zhang, Science **367**, 895 (2020).
[24] Q. L. He, L. Pan, A. L. Stern, E. C. Burks, X. Che, G. Yin, J. Wang, B. Lian, Q. Zhou, E. S. Choi *et al.*, Science **357**, 294 (2017).
[25] L. Zhang, J. Ren, J.-S. Wang, and B. Li, Phys. Rev. B **87**, 144101 (2013).
[26] A. Mook, J. Henk, and I. Mertig, Phys. Rev. B **90**, 024412 (2014).
[27] R. Chisnell, J. S. Helton, D. E. Freedman, D. K. Singh, R. I. Bewley, D. G. Nocera, and Y. S. Lee, Phys. Rev. Lett. **115**, 147201 (2015).
[28] F.-Y. Li, Y.-D. Li, Y. B. Kim, L. Balents, Y. Yu, and G. Chen, Nat. Commun. **7**, 12691 (2016).
[29] E. Prodan and C. Prodan, Phys. Rev. Lett. **103**, 248101 (2009).
[30] L. Zhang, J. Ren, J.-S. Wang, and B. Li, Phys. Rev. Lett. **105**, 225901 (2010).
[31] Y. Jin, R. Wang, and H. Xu, Nano Lett. **18**, 7755 (2018).
[32] S. Park and B.-J. Yang, Phys. Rev. B **99**, 174435 (2019).
[33] G. Go, S. K. Kim, and K.-J. Lee, Phys. Rev. Lett. **123**, 237207 (2019).
[34] S. Zhang, G. Go, K.-J. Lee, and S. K. Kim, Phys. Rev. Lett. **124**, 147204 (2020).
[35] X. Zhang, Y. Zhang, S. Okamoto, and D. Xiao, Phys. Rev. Lett. **123**, 167202 (2019).
[36] S. Park, N. Nagaosa, and B.-J. Yang, Nano Lett. **20**, 2741 (2020).
[37] R. Takahashi and N. Nagaosa, Phys. Rev. Lett. **117**, 217205 (2016).
[38] K. Di, V. L. Zhang, H. S. Lim, S. C. Ng, M. H. Kuok, J. Yu, J. Yoon, X. Qiu, and H. Yang, Phys. Rev. Lett. **114**, 047201 (2015).

[39] S. Tacchi, R. E. Troncoso, M. Ahlberg, G. Gubbiotti, M. Madami, J. Åkerman, and P. Landeros, Phys. Rev. Lett. **118**, 147201 (2017).
[40] A. Qaiumzadeh, I. A. Ado, R. A. Duine, M. Titov, and A. Brataas, Phys. Rev. Lett. **120**, 197202 (2018).
[41] L. Zhang and Q. Niu, Phys. Rev. Lett. **112**, 085503 (2014).
[42] L. Zhang and Q. Niu, Phys. Rev. Lett. **115**, 115502 (2015).
[43] See Supplemental Material at http://link.aps.org/supplemental/10.1103/PhysRevB.105.L100402 for details on model derivations and the numerical method.
[44] T. Moriya, Phys. Rev. **120**, 91 (1960).
[45] T. Moriya, Phys. Rev. Lett. **4**, 228 (1960).
[46] Y. A. Bychkov, JETP Lett. **39**, 78 (1984).
[47] A. Manchon, H. C. Koo, J. Nitta, S. Frolov, and R. Duine, Nat. Mater. **14**, 871 (2015).
[48] L. Sheng, D. N. Sheng, and C. S. Ting, Phys. Rev. Lett. **96**, 155901 (2006).
[49] Y. Kagan and L. A. Maksimov, Phys. Rev. Lett. **100**, 145902 (2008).
[50] J.-S. Wang and L. Zhang, Phys. Rev. B **80**, 012301 (2009).
[51] H. Chen, Q. Niu, and A. H. MacDonald, Phys. Rev. Lett. **112**, 017205 (2014).
[52] M.-T. Suzuki, T. Koretsune, M. Ochi, and R. Arita, Phys. Rev. B **95**, 094406 (2017).
[53] A. Mook, J. Henk, and I. Mertig, Phys. Rev. B **99**, 014427 (2019).
[54] T. Holstein and H. Primakoff, Phys. Rev. **58**, 1098 (1940).
[55] A. G. Del Maestro and M. J. Gingras, J. Phys.: Condens. Matter **16**, 3339 (2004).
[56] R. Shindou, R. Matsumoto, S. Murakami, and J.-i. Ohe, Phys. Rev. B **87**, 174427 (2013).
[57] X.-L. Qi, T. L. Hughes, and S.-C. Zhang, Phys. Rev. B **78**, 195424 (2008).
[58] T. Fukui, Y. Hatsugai, and H. Suzuki, J. Phys. Soc. Jpn. **74**, 1674 (2005).
[59] R. Barnett, G. R. Boyd, and V. Galitski, Phys. Rev. Lett. **109**, 235308 (2012).
[60] B. A. Bernevig, T. L. Hughes, and S.-C. Zhang, Science **314**, 1757 (2006).
[61] C. L. Kane and E. J. Mele, Phys. Rev. Lett. **95**, 226801 (2005).
[62] S. K. Kim, H. Ochoa, R. Zarzuela, and Y. Tserkovnyak, Phys. Rev. Lett. **117**, 227201 (2016).
[63] B. A. Bernevig, *Topological Insulators and Topological Superconductors* (Princeton University Press, Princeton, NJ, 2013).
[64] A. Wildes, B. Roessli, B. Lebech, and K. Godfrey, J. Phys.: Condens. Matter **10**, 6417 (1998).
[65] P. A. Joy and S. Vasudevan, Phys. Rev. B **46**, 5425 (1992).
[66] A. Hashemi, H.-P. Komsa, M. Puska, and A. V. Krasheninnikov, J. Phys. Chem. C **121**, 27207 (2017).
[67] D.-H. Kim, M. Haruta, H.-W. Ko, G. Go, H.-J. Park, T. Nishimura, D.-Y. Kim, T. Okuno, Y. Hirata, Y. Futakawa *et al.*, Nat. Mater. **18**, 685 (2019).
[68] A. Fernández-Pacheco, E. Vedmedenko, F. Ummelen, R. Mansell, D. Petit, and R. P. Cowburn, Nat. Mater. **18**, 679 (2019).
[69] I. Appelbaum, H. Drew, and M. Fuhrer, Appl. Phys. Lett. **98**, 023103 (2011).
[70] P. Di Pietro, M. Ortolani, O. Limaj, A. Di Gaspare, V. Giliberti, F. Giorgianni, M. Brahlek, N. Bansal, N. Koirala, S. Oh *et al.*, Nat. Nanotechnol. **8**, 556 (2013).
[71] T. Ozawa, H. M. Price, A. Amo, N. Goldman, M. Hafezi, L. Lu, M. C. Rechtsman, D. Schuster, J. Simon, O. Zilberberg, and I. Carusotto, Rev. Mod. Phys. **91**, 015006 (2019).